Biosensors and Bioelectronics 135 (2019) 192–199

Contents lists available at ScienceDirect

Biosensors and Bioelectronics

journal homepage: www.elsevier.com/locate/bios

Synthesis of wearable and flexible $NiP_{0.1}$-SnO_x/PANI/CuO/cotton towards a non-enzymatic glucose sensor

Ali Sedighi[a], Majid Montazer[b,*], Saeedeh Mazinani[c]

[a] Nanotechnology Institute, Textile Department, Amirkabir University of Technology, Tehran, Iran
[b] Textile Department, Amirkabir Nanotechnology Research Institute (ANTRI), Amirkabir University of Technology, Tehran, Iran
[c] New Technologies Research Center (NTRC), Amirkabir University of Technology, Tehran, Iran

ARTICLE INFO

Keywords:
Glucose sensor
Nickel electroless plating
Flexible wearable sensor
Electrocatalytic activity
Nonenzymatic
Conductive cotton fabric

ABSTRACT

Ni-SnO_x, PANI and CuO nanoparticles were synthesized on cotton fabric through chemical methods to make a new flexible high-performance non-enzymatic glucose sensor. FESEM, XRD, XPS, EDS and ATR analysis were employed to characterize the structure and the morphology of the nanomaterials. The high electrochemical performance of nickel and copper oxide and hydroxide on a conductive template leads to fabrication of a wearable and flexible cotton electrode with an excellent electrocatalytic activity to oxidize glucose. This hybrid system on the fabric as an electrode indicates a detection limit of 130 nM with wide linear range of 0.001–10 mM. The sensitivity was measured to be 1625 and 1325 $\mu A\,mM^{-1}\,cm^{-2}$ for the ranges of 0.001–1 and 1–10 mM, respectively. Long-term stability, appropriate selectivity and reusability for many times make possibility for utilizing the fabricated sensor in the practical applications. The fabric is a wide linear range electrode with low detection limit to sense glucose concentration in the body fluids as well as the human blood that can be presumably suggested for designing other similar flexible types of sensor.

1. Introduction

Glucose monitoring is essential in order to reduce the risk of diabetes, a metabolic disorder caused by the insulin deficiency. 422 millions of people around the world suffer from diabetes according to WHO recent report (Organization, 2016). Increasing the glucose levels in blood may lead to retinopathy, renal disease, non-healing wounds, cardiovascular disease and neurological disorders depending on health level, location and other conditions (Witkowska Nery et al., 2016). Therefore, urgent requirements to diagnose diabetes at early stages lead to more research every year in promoting glucose sensors with high sensitivity, selectivity and stability.

Great selectivity is the main factor in developing enzymatic glucose sensor using glucose oxidase (GOx) as usual. However, the poor thermal and chemical stability and high cost has restricted the enzymatic sensors (Chaiyo et al., 2018). Overcoming the limitations, non-enzymatic glucose sensors have been developed based on direct electrocatalytic oxidation using metals, metal alloys and metal oxides nanoparticles (Dong et al., 2018).

Nickel nanoparticles as a transition metal with good stability and reproducibility is one of the best candidate for construction of electrode for glucose electrochemical detection. Nickel compound nanomaterials are highly regarded due to their considerable redox behavior (Ni^{2+}/Ni^{3+}), high surface area and high conductivity of their metallic form. Additionally, Ni electrode is more cost effective than noble metals makes it appropriate for the development of enzyme-free glucose sensors. Copper-based nanostructures with good tunability and desirable electrocatalytic activity for glucose oxidation has also been considered, recently (Dayakar et al., 2018). Utilizing copper oxide as a p-type semiconductor with nickel nanomaterials as a conducting metal lead to better sensitivity and conductivity for electrocatalytic process (Zhang et al., 2014).

Combination of nickel and copper oxide nanoparticles requires strong interactions between them. To promote copper nanoparticles stabilization and distribution on the nickel surface, polymers can be employed. On the other hand, required electrical conductivity restricted the polymer selection into electrically conductive polymers. Polyaniline (PANI) has many applications in sensor fields due to its π-conjugated backbone which facilitates electron transfer and easy doping capability (Lai et al., 2016). PANI is stable in air, biocompatible and not expensive (Lai et al., 2016). It acts not only as a template for immobilizing copper oxide nanoparticles but also improves the electrical properties of composite in addition to higher loading of metal oxide nanoparticles.

In recent years, great attention has been paid to wearable and

* Corresponding author. Textile Department, Nanotechnology Research Institute (ANTRI), Amirkabir University of Technology, Tehran, Iran.
E-mail address: tex5mm@aut.ac.ir (M. Montazer).

https://doi.org/10.1016/j.bios.2019.04.010
Received 1 December 2018; Received in revised form 3 March 2019; Accepted 5 April 2019
Available online 10 April 2019
0956-5663/

mechanical flexible devices including wearable glucose sensors. Enzymatic wearable and flexible glucose sensors have some problems including deactivation of enzymes by temperature, pH and scouring in addition to shelf-life decreasing and degradation with time. Furthermore, immobilizing of enzymes on the wearable substrate reduces the conductivity and thus the electron transfer influencing the enzymes effectiveness (Chaiyo et al., 2018). Cotton fabric as a natural hydrophilic template with high porosity and wettability allows glucose the access to a huge number of catalytic and electroactive sites to enhance redox process and electrochemically glucose detection, consequently. Employing cotton fabric as a flexible template with active functionality for wearable sensor not only improves the stability of the glucose sensor by allowing the nanomaterials to interacts chemically to the substrate, but also endows the flexibility, biocompatibility and comfortability to the sensor. Using a flexible wearable substrate without using binder results in higher porosity, stability and electrocatalytic performance of electrode for glucose detection.

In the present work, $NiP_{0.1}$-SnO_x/PANI/CuO (NTPC) nanocomposite were synthesized and deposited on cotton fabric. $NiP_{0.1}$-SnO_x particles were in situ synthesized through nickel electroless plating on catalytically nickel-activated fabric. In order to immobilize the copper oxide on the fabric and improving ion transfer on the surface, PANI was in-situ synthesized using chemical method on treated fabric. Copper oxide was also synthesized separately and the fabric deposition was carried out through soaking process. The formation mechanism and the synthesis process have been discussed in details in the rest of manuscript. The NTPC cotton fabric electrode was utilized for non-enzymatic glucose detection exhibiting high sensitivity, wide linear range, acceptable reproducibility, reasonable selectivity and low detection limit.

2. Results and discussion

2.1. Synthesis and characterization

The synthesis mechanism was described in supplementary section. The scheme of the fabrication of NTPC electrode including activation, Ni-P electroless plating, PANI polymerization and CuO synthesis is depicted in Fig. 1.

XRD spectra of coated fabric with $NiP_{0.1}$-SnO_x/PANI (NTP) is shown in Fig. 2a. The diffraction peak at $2\theta = 22.9^\circ$ is attributed to the cellulosic fabric crystal (JCPDS 03–0226). The broad diffraction peak at 44.0° confirms nickel nanoparticles synthesis aligned with (1 1 1) crystallographic planes (JCPDS 89–7128). The other weak peaks at 30.66 and 52.5° correspond to SnO (1 0 1) and SnO_2 (2 1 1), respectively (JCPDS 77–0451). The crystallites' size of nickel nanoparticles was calculated to be 3 nm from the widths of the peak at 44.0° using FWHM in Scherrer equation.

The XRD pattern of NTPC on fabric is illustrated in Fig. 2a. The stronger peaks at 22.6 and 44.4° at 2θ are for cotton fabric and nickel (1 1 1) nanoparticles, respectively. There are also small diffraction peaks at $2\theta = 35.6$, 38.9 and 61.7° related to the cupric oxide nanoparticles corresponding to ($\bar{1}$ 1 1), (1 1 1) and (3 1 1) planes (JCPDS 05–0661). Also some shifts and alterations were observed related to tin compounds. The average crystallite' size of the cupric oxide on the fabric was calculated to be 11 nm by Debye-Scherrer equation.

Fig. 2b shows ATR spectra of NTPC electrode. The peaks at 762 cm^{-1} is ascribed to out of plane bending of C-H in PANI and also the chlorine doped with PANI (Trchová and Stejskal, 2011). The bending of C-O-P is observed at 966 cm^{-1} or it may be due to the stretching vibration of S=OR groups on the surface (Field et al., 2012; Zou et al., 2016). The peaks located at 1493 and 1740 cm^{-1} are attributed to the stretching vibration of benzene ring of PANI and C=O stretching vibration of cellulosic fiber (Field et al., 2012; Zou et al., 2016). C-H bending of aromatic compounds of PANI are identified at 1867 and 1927 cm^{-1} (Field et al., 2012). It also may be related to stretching of carbonyl groups (Field et al., 2012). The absorption band assigned to C=C=N stretching vibration on cotton fiber is located in 1979 cm^{-1} (Field et al., 2012). The peaks at 2158, 2249 and 2312 cm^{-1} are the characteristic of stretching vibrations of C=C=O, N=C=O and O=C=O bonds, respectively (Field et al., 2012). The absorption peaks at 2690 and 2940 cm^{-1} are attributed to the cellulose C-H stretching vibration and/or O-H stretching bond on the fabric (Gantner et al., 1994; Trchová and Stejskal, 2011). Several peaks in the range of 3000–3500 cm^{-1} are assigned to hydroxyl stretching vibration and amine groups (Sedighi and Montazer, 2016; Sedighi et al., 2014b). The peaks at 3531 and 3720 cm^{-1} are ascribed to intermolecular and free O-H stretching bond respectively (Sedighi et al., 2014a).

NTP coating on the fabric surface is exhibited in Fig. 3a and b. Huge amount of aggregated and agglomerated nickel-phosphorous particles doped with SnO and SnO_2 nanoparticles were synthesized and coated on the fabric surface. Some places on the fabric where NiP-SnO_x particles are not present, PANI nanoparticles can be seen on the surface. Unlike Ni-P particles, spherical PANI nanoparticles have more uniform and less complex distribution on the substrate surface. This is because magnetic forces between nickel particles contributed to attract forces and nanoparticles rapid aggregation. Huge amount of deposition also increased the agglomeration and aggregation possibility. The presence of nickel particles and their position on the surface depends exactly on the activation process in which in-situ synthesis and deposition of nickel nanoparticles on the fabric surface was carried out. Cotton fabric as a cellulosic material has many active hydroxyl groups on its surface. These functional groups besides a large number of defects on the fiber surface allows formation of many nucleation sites on the fabric surface. Electroless deposition of NiP-SnO_x nanoparticles on the fabric surface was exactly carried out on the nickel particles on fabric surface. Nickel nanoparticles on the fabric surface determine the positions of synthesized nickel-phosphorous particles besides the tin oxide nucleation and additionally accelerate the electroless plating acting as a catalyst. Hence, the uniformity of particles distributions depends on the prior catalytic activation of the fabric with nickel nanoparticles. The more primary nickel nanoparticles deposition, the more nickel-phosphorous with more uniform deposition on the fabric surface.

Another factor influencing the nickel particles morphology on the fabric surface is temperature. Since the deposition rate on the surface depends on the electroless plating process temperature. The deposition rate can also control the particles' and aggregation size. pH of the electroless plating bath is another important factor affecting the thickness and amount of nanoparticles as well as their size on the fabric. More comprehensive images of nanoparticle coating on the fibers is illustrated in Fig. 1Sa and Sb. Cupric oxide nanoparticles distribution on the treated fabric is exhibited in Fig. 3c and d. Cupric oxide nanoparticles are deposited between NiP-SnO_x aggregates and PANI nanoparticles. The amount of copper oxide will be increased on the surface with increasing the number of fabric immersions as well as growing the immersion time duration. Enhancing the heat setting temperature also has positive impact on stronger interactions between particles and treated fabric.

EDX analysis (Table S1) shows elemental amount within a specified place on the fabric surface. 40.2% is the nickel amount after final coating with cupric oxide (NTPC electrode). The amount of phosphorous is 19.1 and 15.9% before and after cupric oxide coating, respectively. Chlorine, sulfur and nitrogenous compounds were also deposited during electroless plating on the fabric in addition to the $NiP_{0.1}$-SnO_x particles. These elements played an important role in the interactions between nickel, copper oxide, PANI and cellulosic fabric. The tin content was 9.7% for NTP which was decreased to 6.9% after copper oxide deposition. Copper content on the fabric is sensible for copper oxide treated fabric (4.3%) according to add-on. In addition, nitrogen decrease detected as part of PANI or/and nickel-phosphorous coating in NTP, indicated the nitrogen positive influence in copper adsorption within copper oxide deposition. In order to clarify the mentioned issue, cupric oxide was deposited on a NiP-SnO_x coated fabric without PANI

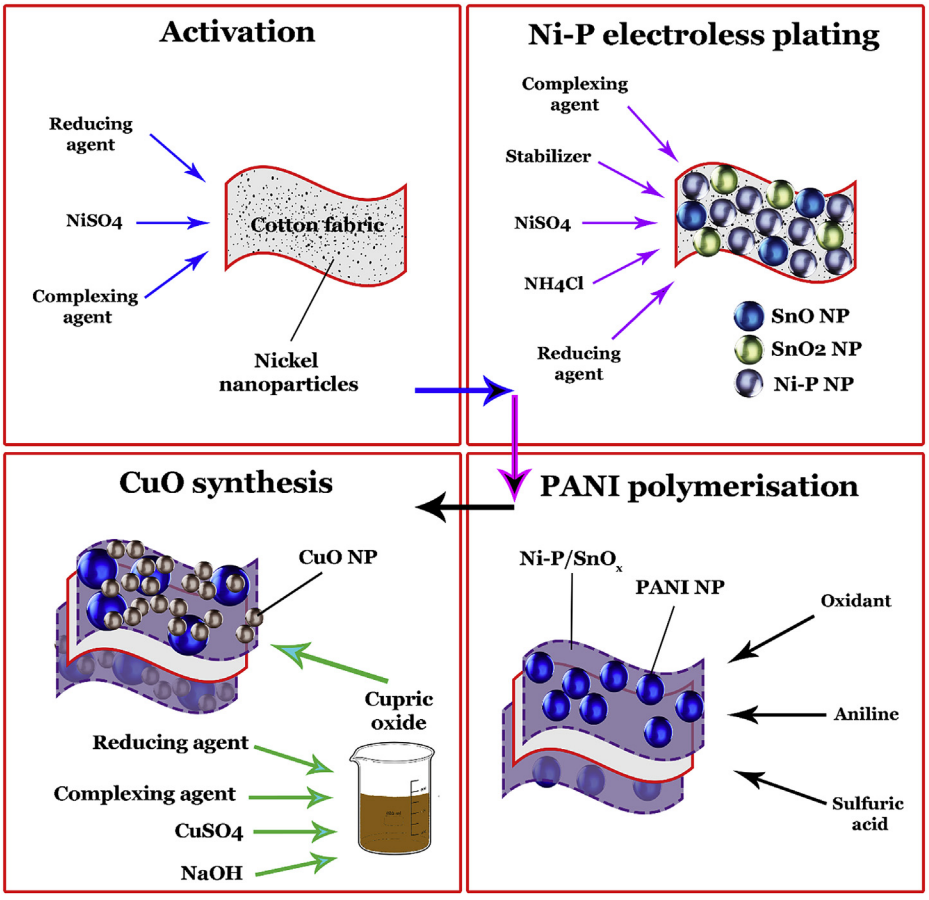

Fig. 1. The fabrication Schematic of NTPC electrode.

to confirm the PANI role in cupric oxide deposition. The elemental analysis displays that the copper oxide absorption on the surface decreased to 3.5% as can be observed in FESEM images in Fig. S1c and 1d. As a result, PANI acts as a template to enhance the interactions between copper oxide and the treated fabric due to the oxidize form of polymer chains (Gautam et al., 2018). The corresponding EDS color mappings of elements of the NTPC electrode are exhibited in Fig. S2.

The synthesis of NTPC on cellulosic fabric was further characterized by XPS analysis. Fig. 4 exhibits XPS survey spectrum of the coated substrate. The asymmetric peaks at 135, 168, 285, 400, 487, 532, 856, 933 and 1071 eV correspond to the P 2p, S 2p, C 1s, N 1s, Sn 3d, O 1s, Ni 2p, Cu 2p and Na 1s, respectively.

The Sn 3d spectra shows two peaks at 484.9 and 493.3 eV ascribed to Sn $3d_{5/2}$ and $3d_{3/2}$ corresponding to metalized tin, respectively (Kövér et al., 1995a; Ohno, 1991) (Fig. 4b). Chemical state assignment for tin is difficult due to overlapping Sn $3d_{5/2}$ values for SnO and SnO_2 (Süzer, 1997). The peak centered at 487.0 eV corresponds to 3d signals of both SnO_2 and SnO (Schenk-Meuser and Duschner, 1997). The larger peaks at 495.1 and 497.0 eV are related to Sn $3d_{5/2}$ corresponding to Sn^{2+} and Sn^{4+}, respectively (Kövér et al., 1995b). The spin orbital splitting energy of tin cations is 10 eV while there is a combination of Sn, SnO and SnO_2 on the substrate.

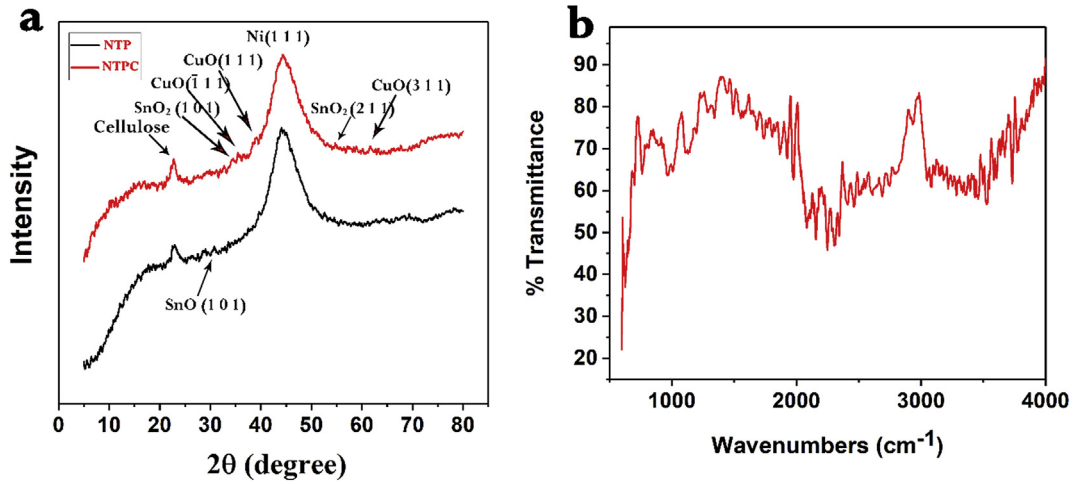

Fig. 2. (a) XRD patterns of NTP and NTPC electrodes and (b) ATR spectra of NTPC electrode.

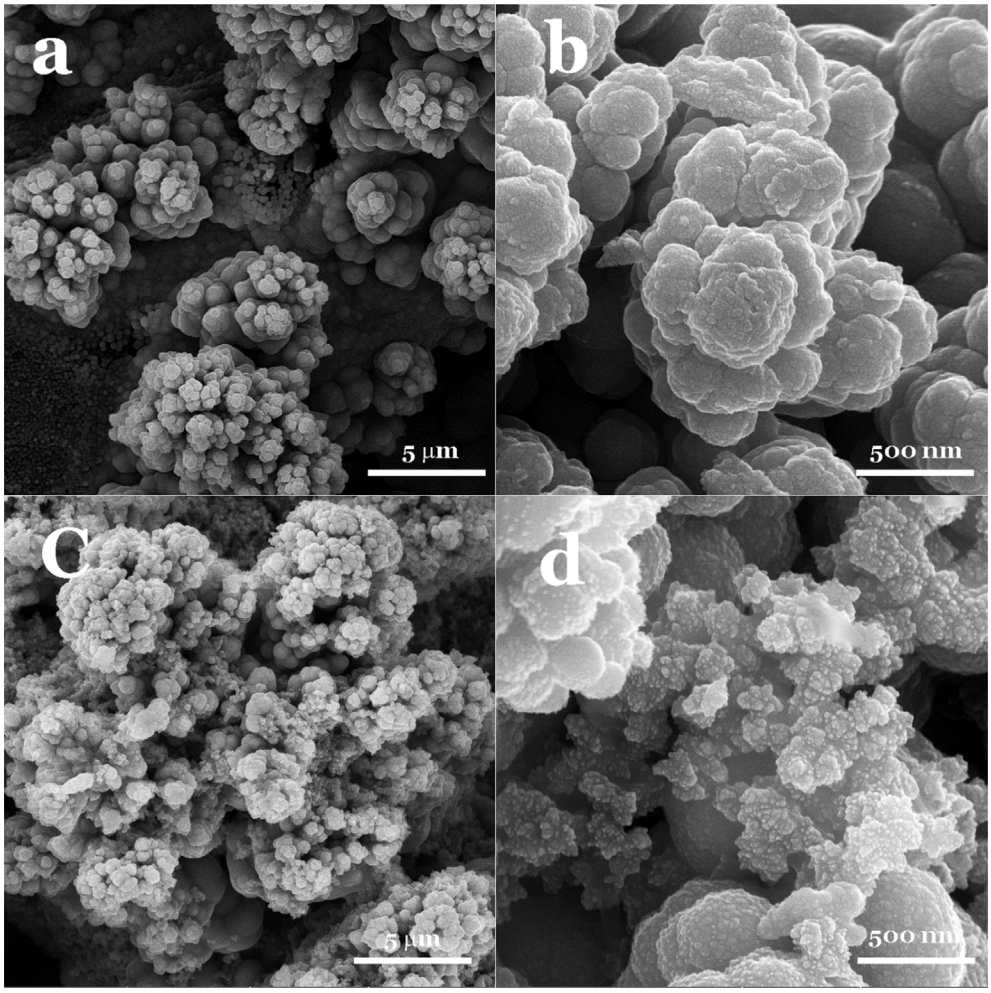

Fig. 3. FESEM images of (a) and (b) NTP and (c) and (d) NTPC electrodes.

The Cu 2p spectra shows peaks at 933.7 and 953.5 eV corresponding to $2p_{3/2}$ and $2p_{1/2}$ signals of copper oxide, respectively (Liu et al., 2016) (Fig. 4c). The satellite peaks 942.1 and 956.8 eV belong to $2p_{3/2}$ and $2p_{1/2}$ (Liu et al., 2016). The binding energy peaks confirms the presence of Cu^{2+} and possibly tangible amount of Cu^0 on the fabric substrate. The spin-energy separation is 19.8 eV. The area ratio for the two spin orbital peaks ($2p_{1/2}$: $2p_{3/2}$) is almost 1:2.

According to Fig. 4d, the peaks confirm dominant $Ni(OH)_2$ on the substrate surface. The deconvoluted peaks at binding energy of 855.9 and 856.6 eV are attributed to Ni $2p_{3/2}$ corresponding to Ni^{2+}, possibly according to NiO and $Ni(OH)_2$ on the fabric surface (Karikalan et al., 2016). The peaks appeared at 861.4 eV is $2p_{3/2}$ shakeup satellite peak of $Ni(OH)_2$(Shu et al., 2018). The nickel metal is also observed in 852.7 eV corresponding to Ni $2p_{3/2}$ (Karikalan et al., 2016). Overlapping of high bonding energy satellite structure from $Ni(OH)_2$ and NiO (to a lesser extent) in $2p_{3/2}$ and $2p_{1/2}$ is possibly occurred. The peaks at 874 and 880 eV ascribed to $2p_{1/2}$ peaks of $Ni(OH)_2$ and $Ni(OH)_2$ satellite peak, respectively.

2.2. Cyclic voltammetry of cotton fabric electrode towards glucose

Cyclic voltammetry was measured to examine the catalytic activity of cotton fabric containing different nanoparticles towards glucose oxidation in an alkaline solution. Fig. 5a and b illustrates the CV curves of Ni-$P_{0.1}/SnO_x$ (NT), $NiP_{0.1}/SnO_x$/CuO (NTC), NTP and NTPC samples in 0.1 M NaOH in the presence and absence of 2 mM glucose at a scan rate of 50 mV/s, respectively. Well-defined redox peaks in all CV curves can be observed. It should be noted that the first cycle of CV is different from the other cycles due to the irreversible oxidation of metallic Ni to Ni^{2+} in the alkaline solution. Part of the high electrochemical behavior of the electrodes relate to the cotton fabric as a porous substrate that hinders close-packed structure of hybrid nanoparticles consequently enhances the specific surface area.

Higher oxidation and reduction potential current peaks are attributed to NTPC and NT electrodes. The peak current of NT is the highest even higher than NTPC. The better electrochemical performance of NT is possibly due to the more electrical conductivity compared to the other electrodes. On the other hand, the more content with lower compactness of nickel particles on the surface compared to that of the fabrics coated with PANI or/and cupric oxide besides nickel particles are the other reasons to explain the higher anodic peak for NT in the alkaline condition without glucose.

The oxidation current of all the samples were enhanced after adding 2 mM glucose as shown in Fig. 5b. This is because of the electro-oxidation of glucose with the catalytic behavior of Ni(III) and Cu(III). The current of oxidation peaks increased and the reduction peaks current decreased with adding glucose to NaOH solution in the presence of NTPC. The redox peaks were observed at potentials of 0.62 and 0.35 which was affected by the redox couples of Ni(II) to Ni(III) and Cu(II) to Cu(III) in alkaline solution according to reactions 8–11.

$$Ni(OH)_2 + OH^- \rightarrow NiO(OH) + H_2O + e^- \quad (8)$$

$$NiO(OH) + \text{glucose} \rightarrow Ni(OH)_2 + H_2O + \text{gluconolactone} \quad (9)$$

$$CuO + OH^- \rightarrow CuO(OH) + e^- \quad (10)$$

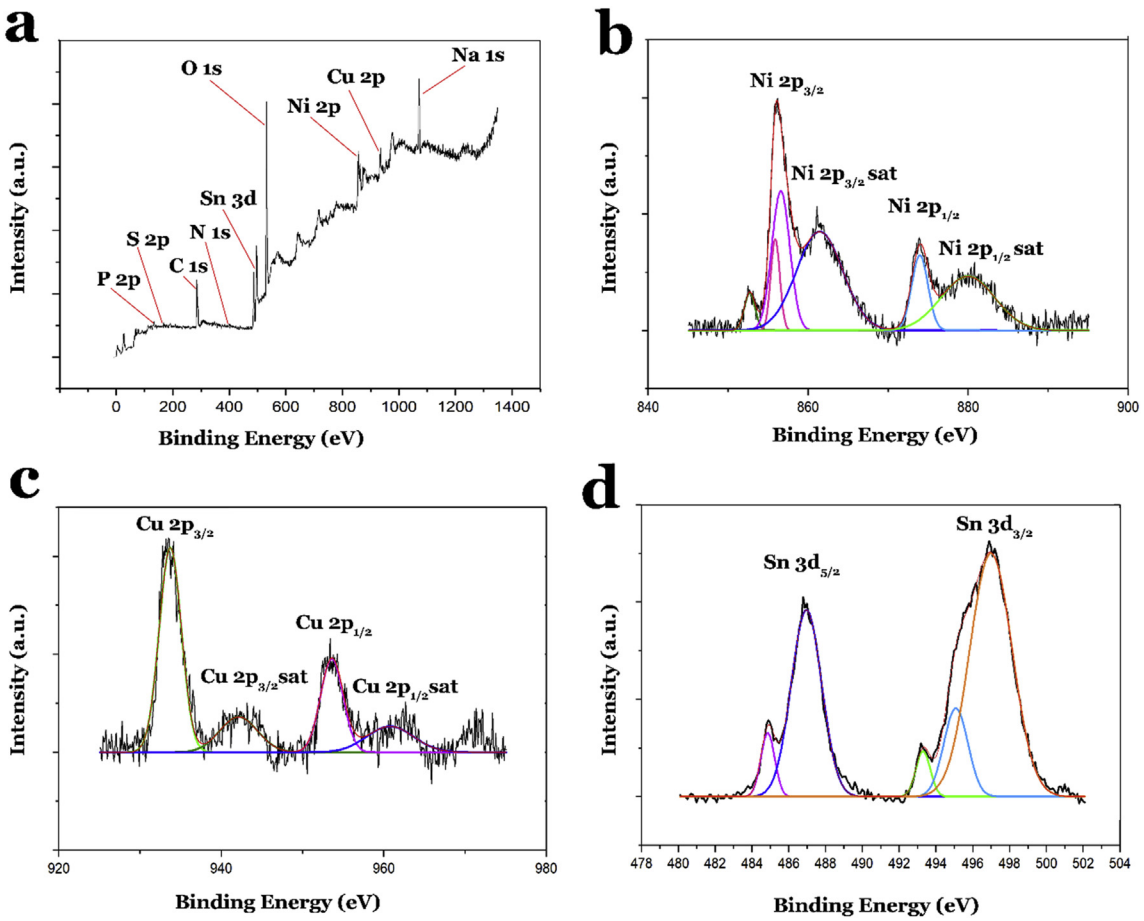

Fig. 4. (a) XPS survey spectrum, and (b) Ni 2p, (c) Cu 2p, and (d) Sn 3d spectra obtained for NTPC electrode.

$$CuO(OH) + e^- + glucose \rightarrow CuO + OH^- + gluconolactone \quad (11)$$

Close oxidation and reduction peaks of Ni(II) and Cu(II) causes the most electrocatalytic enhancement for NTPC among other electrodes. This attributes to the overlapping of the redox peaks and thus the synergistic electrocatalytic performance of them. Furthermore, PANI bonding with nickel particles and cotton fabric facilitates immobilizing of copper oxide nanoparticles on the surface. These reasons cause a higher peak current for NTPC comparing with the other electrodes.

The glucose sensing characteristics of NTPC electrode were furtherly examined at glucose concentrations ranging from 0.2 to 5 mM at a scan rate of 50 mV/s (Fiure 5c). Increasing the glucose concentration within 0.2–5 mM enhances the oxidation current peaks of NTPC as exhibited in Fig. 5c. Also, the cathodic peak current signals slightly increases as the glucose concentration rises. The remarkable anodic peak shifts to the higher potentials possibly attributed to the diffusion limitation of glucose (Kannan et al., 2016) as well as electrocatalysis activity of $Ni(OH)_2$ on glucose oxidation at the electrode surface.

The effect of scan rate on the glucose oxidation on NTPC electrode in 0.1 M NaOH and 1 mM glucose is depicted in Fig. 5d. The anodic peak increased and the cathodic peak shifted to the lower potentials with increasing the scan rate because of the slower reaction kinetics of the electrocatalytic processing within the glucose adsorption at the higher scan rates. Anodic peak currents shifted to the more positive potentials and the cathodic peak currents moved to the lower positive potentials according to Fig. 5c. The oxidation and reduction peak currents were both proportional to the square root of the scan rates within 10–100 mV/s with correlation coefficient (R^2) of 0.955 and 0.963, respectively (Fig. S4a). It is concluded that the glucose redox reaction is a diffusion-controlled process makes the glucose sensor practical for quantitative analysis.

2.3. Amperometric response of NTPC electrode towards glucose

Fig. 6a expresses the amperometric response of NTPC electrode to the stepwise addition of glucose into the stirred 100 mM NaOH solution at 0.65 V working potential. The detection potential was determined 0.65 V in which NTPC electrode has the best obvious current response upon the stepwise glucose addition according to the investigation in other voltages, 0.55 and 0.6 V, to obtain better glucose detection for anodic increase.

The electrode responded immediately after injecting given concentrations of glucose solution into the NaOH alkaline solution and a change in current towards a steady state was observed after each addition. The glucose sensing behavior of NTPC electrode was examined at the range of 0.05μM–10 mM with scan rate of 30 mV/s in NaOH solution. The response time towards the oxidation of glucose is almost 3 s indicating a fast response according to Fig. S4b.

The calibration curve in Fig. 6b over the range from 1 to 1000 μM glucose concentration is obtained to be linear. At glucose concentration from 1 to 1000 μM, the response equation is I(mA) = 0.0005C(μM) + 0.5778 with correlation coefficient of 0.999. The NTPC fabric is highly suited for non-enzymatic glucose sensor in sweat, saliva and even tears due to its excellent linear calibration curve where the glucose concentration is within 1–1000 μM.

The sensor sensitivity was calculated to be 1625 $\mu A\, mM^{-1}\, cm^{-2}$. Moreover, the linearity of current response with glucose concentration in the range of 1–10 mM is considerably close to the level of actual blood glucose level (4–8 mM). It was determined with correlation

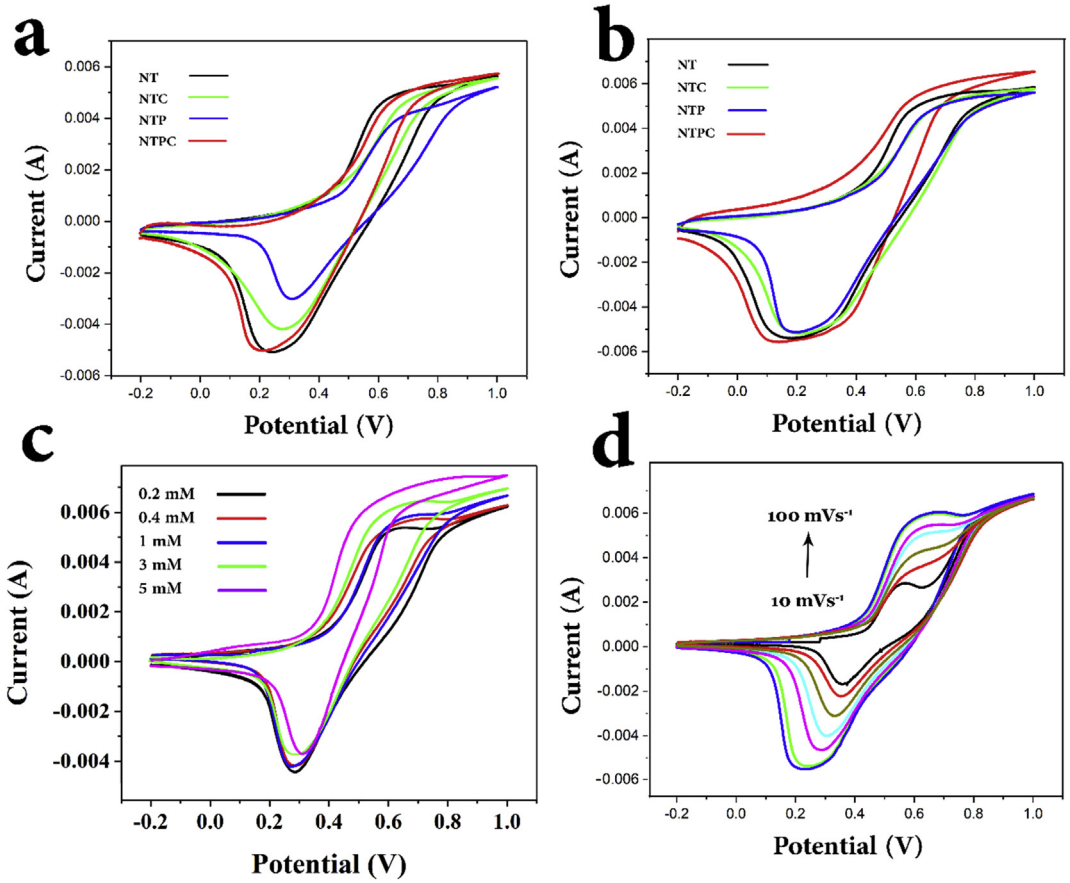

Fig. 5. (a) CV curves of NT, NTC, NTP and NTPC in 0.1 M NaOH without glucose and (b) with 2 mM glucose at a scan rate of 50 mV/s. (c) Typical CV curves of NTPC in the presence of different concentrations (0.2, 0.4, 1, 3 and 5 mM) of glucose in 0.1 M NaOH at a scan rate of 50 mV/s (d) CV curves of NTPC in 0.1 M NaOH at different scan rates including; 10, 20, 30, 40, 60, 90 and 100 mV/s.

coefficient of 0.9936 (Fig. 4Sc) with the response equation of I (mA) = 0.0004C(μM) + 1.3658. This demonstrates that there are still more active sites on the fabric electrode to bind with glucose even after 10 mM concentration. However, the linearity decreased slightly in higher concentration. Fig. 6b inset confirmed the linearity of the sensor's amperometric detection of glucose concentration with 0.9963 correlation coefficient within 1–10000 μM. Such a wide linear range is ideal for applicable glucose sensor. The sensitivity was obtained 1325 and 1355 $\mu A\, mM^{-1}\, cm^{-2}$ in 1–10 and 0.001–10 mM glucose concentrations, respectively. It should be noted that cotton fabric roles in increasing the dispersity of nanoparticles on the substrate leads to the higher sensitivity of the electrode due to the increase in accessible specific surface area.

According to the sensitivity, the detection limit of NTPC sensor was determined to be 130 nM based on a signal to noise ratio 3, which is suggesting a low detection limit among the other reported non-enzymatic glucose sensor (Fig. 6c). 130 nM glucose was injected into NaOH solution causes the current increased, almost 19 nA comparing with the previous current.

The selectivity of NTSC sensor was determined by adding possible interfering compounds including NaCl, ascorbic acid, urea and uric acid which coexist with glucose in the human blood to NTPC sensor. Addition of 1 mM glucose was followed by inserting 0.1 mM urea, uric acid, ascorbic acid and NaCl at 0.65 V (Fig. 6d) considering the fact that glucose concentration in blood is 30 times more than these interfering compounds (Zhang et al., 2014). Unlike the interfering agents, a remarkable glucose response observed suggesting considerable specificity of NTPC electrode for enzymeless glucose detection with coexisting interfering materials. The comparison of the sensing properties including detection limit, linear range and sensitivity of some of the previous reported sensors based on CuO and Ni compounds electrodes are included in Table 1.

To evaluate the practical application of the sensor, the stability and reusability of the fabricated electrode was tested by measuring the current alternatively within a week according to Fig. S4d. After 7 times amperometry test every day, the current response of the electrode shows approximately 10% reduction compared to the original amperometric response. Thus, the fabric has the ability to be reused for glucose detection for many times with an appropriate stability.

3. Conclusion

A wearable and flexible textile-based electrode was fabricated for non-enzymatic glucose detection utilizing $NiP_{0.1}/SnO_x$/PANI/CuO nanomaterials on cotton fabric substrate using facile chemical synthesis methods. In order to make the fabric electrically conductive, it was activated using nickel nanoparticles as catalyst prior to nickel electroless plating. Growth of nickel nanoparticles directly on the cotton surface and CuO nanoparticles deposition on the treated fabric leads to fabrication of a developed hybrid nanostructure system with high electrochemical activity which originates from the combination of materials with efficient highly electrocatalytic behavior (CuO and Ni). Coating PANI on phosphorous doped nickel nanoparticles allows CuO nanoparticles to more deposition on the fabric surface taking advantages of better electron transfer acceleration. The NTPC electrode indicates a remarkable electrocatalysis behavior in a wide linear range of 0.001–10 mM with low detection limit of 130 nm and fast response comparing to the other previously reported sensors. The sensitivity of

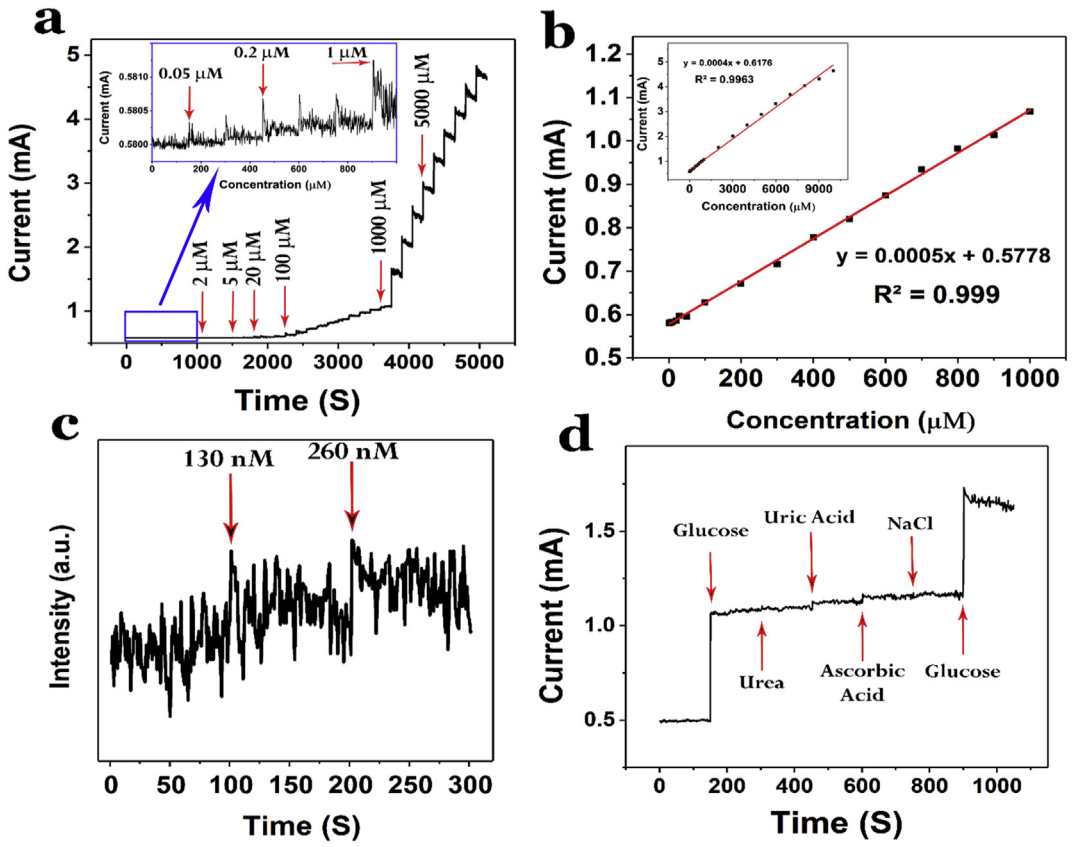

Fig. 6. (a) Amperometric response of the NTPC electrode with stepwise addition of glucose to 0.1 M NaOH solution at regular intervals. The applied potential was +0.65 V. (b) Corresponding calibration curve of the NTPC glucose sensor in the range of 0.001–1 mM, the inset is a linear regression of total glucose concentration (0.1–10 mM). (c) Amperometric response of the electrode with the successive addition of 130 nM glucose into the solution. (d) Amperometric response to the stepwise injection of 1.0 mM glucose, 100 mM urea, 100 mM uric acid, 100 mM ascorbic acid and 100 mM NaCl, followed by the successive addition of 1.0 mM glucose.

Table 1
Comparison of the performance of various Ni—and CuO-based nonenzymatic glucose sensors.

Electrode	Linear range (mM)	Detection limit (mM)	Sensitivity ($\mu A mM^{-1} cm^{-2}$)	Ref.
CuO nanocubes-graphene	2–4	0.7	1360	Luo et al. (2012)
CuO/MWCNTs	3	0.8	2190	Yang et al. (2010)
CeO_2@CuO	0.001–0.0089	0.019	3319.83	Dayakar et al. (2018)
GM-NiO	1–100	1.6	918	Liu et al. (2014)
RGO-$Ni(OH)_2$/GCE	0.002–3.1	0.6	1143	Zhang et al. (2011)
$Ni(OH)_2$/3DGF	1–1.17	0.34	2650	Zhan et al. (2014)
$NiCo_2S_4$	250–2000	0.55	858.57	Chen et al. (2017)
Pt–NiO/rGO/GCE	0.008–14.5	2.67	832.95	Wang et al. (2015)
NiO nanoparticle/GO/GCE	0.00313–3.05	1.0	1087	Yuan et al. (2013)
Cu_2O–CLGNs/GCE	0–10	1.83	1215.7	Chen et al. (2015)
Ni-SnO_x/PANI/CuO	0.001–1; 1-10	0.130	1625; 1325	This work

Synthesis of wearable and flexible $NiP_{0.1}$-SnO_x/PANI/CuO/Cotton towards a non-enzymatic glucose sensor.

1625 and 1325 $\mu A\, mM^{-1}\, cm^{-2}$ was obtained for two linear ranges for glucose detection. Moreover, the fabricated modified sensor suggests an excellent selectivity with long-term stability as well as considerable reusability towards applicable glucose sensors.

CRediT authorship contribution statement

Majid Montazer: Supervision, Writing - review & editing. **Saeedeh Mazinani:** Supervision.

Appendix A. Supplementary data

Supplementary data to this article can be found online at https://doi.org/10.1016/j.bios.2019.04.010.

References

Chaiyo, S., Mehmeti, E., Siangproh, W., Hoang, T.L., Nguyen, H.P., Chailapakul, O., Kalcher, K., 2018. Non-enzymatic electrochemical detection of glucose with a disposable paper-based sensor using a cobalt phthalocyanine–ionic liquid–graphene composite. Biosens. Bioelectron. 102, 113–120.

Chen, A., Ding, Y., Yang, Z., Yang, S., 2015. Constructing heterostructure on highly roughened caterpillar-like gold nanotubes with cuprous oxide grains for ultrasensitive and stable nonenzymatic glucose sensor. Biosens. Bioelectron. 74, 967–973.

Chen, D., Wang, H., Yang, M., 2017. A novel ball-in-ball hollow NiCo 2 S 4 sphere based sensitive and selective nonenzymatic glucose sensor. Anal. Methods 9 (32), 4718–4725.

Dayakar, T., Rao, K.V., Bikshalu, K., Malapati, V., Sadasivuni, K.K., 2018. Non-enzymatic sensing of glucose using screen-printed electrode modified with novel synthesized

CeO2@ CuO core shell nanostructure. Biosens. Bioelectron. 111, 166–173.
Dong, Q., Huang, Y., Song, D., Wu, H., Cao, F., Lei, Y., 2018. Dual functional rhodium oxide nanocorals enabled sensor for both non-enzymatic glucose and solid-state pH sensing. Biosens. Bioelectron. 112, 136–142.
Field, L.D., Sternhell, S., Kalman, J.R., 2012. Organic Structures from Spectra. John Wiley & Sons.
Gantner, E., Beck, M., Müller, H., Steinert, D., Ache, H., 1994. Process analysis of electroless nickel deposition baths by Raman spectroscopy. J. Raman Spectrosc. 25 (1), 31–41.
Gautam, V., Singh, K.P., Yadav, V.L., 2018. Polyaniline/multiwall carbon nanotubes/starch nanocomposite material and hemoglobin modified carbon paste electrode for hydrogen peroxide and glucose biosensing. Int. J. Biol. Macromol. 111, 1124–1132.
Kannan, P., Maiyalagan, T., Marsili, E., Ghosh, S., Niedziolka-Jönsson, J., Jönsson-Niedziolka, M., 2016. Hierarchical 3-dimensional nickel–iron nanosheet arrays on carbon fiber paper as a novel electrode for non-enzymatic glucose sensing. Nanoscale 8 (2), 843–855.
Karikalan, N., Velmurugan, M., Chen, S.-M., Karuppiah, C., 2016. Modern approach to the synthesis of Ni (OH) 2 decorated sulfur doped carbon nanoparticles for the nonenzymatic glucose sensor. ACS Appl. Mater. Interfaces 8 (34), 22545–22553.
Kövér, L., Kovács, Z., Sanjinés, R., Moretti, G., Cserny, I., Margaritondo, G., Pálinkás, J., Adachi, H., 1995a. Electronic structure of tin oxides: high-resolution study of XPS and Auger spectra. Surf. Interface Anal. 23 (7-8), 461–466.
Kövér, L., Moretti, G., Kovács, Z., Sanjinés, R., Cserny, I., Margaritondo, G., Pálinkás, J., Adachi, H., 1995b. High resolution photoemission and Auger parameter studies of electronic structure of tin oxides. J. Vac. Sci. Technol. Vacuum Surf. Films 13 (3), 1382–1388.
Lai, J., Yi, Y., Zhu, P., Shen, J., Wu, K., Zhang, L., Liu, J., 2016. Polyaniline-based glucose biosensor: a review. J. Electroanal. Chem. 782, 138–153.
Liu, J., Lv, W., Wei, W., Zhang, C., Li, Z., Li, B., Kang, F., Yang, Q.-H., 2014. A three-dimensional graphene skeleton as a fast electron and ion transport network for electrochemical applications. J. Mater. Chem. 2 (9), 3031–3037.
Liu, S., Hui, K., Hui, K., 2016. Flower-like copper cobaltite nanosheets on graphite paper as high-performance supercapacitor electrodes and enzymeless glucose sensors. ACS Appl. Mater. Interfaces 8 (5), 3258–3267.
Luo, L., Zhu, L., Wang, Z., 2012. Nonenzymatic amperometric determination of glucose by CuO nanocubes–graphene nanocomposite modified electrode. Bioelectrochemistry 88, 156–163.
Ohno, Y., 1991. Electronic structure of the misfit-layer compounds PbTiS 3 and SnNbS 3. Phys. Rev. B 44 (3), 1281.
Organization, W.H., 2016. Global Report on Diabetes. World Health Organization.
Schenk-Meuser, K., Duschner, H., 1997. ESCA-analysis of tin compounds on the surface of hydroxyapatite. Fresenius J. Anal. Chem. 358 (1–2), 265–267.
Sedighi, A., Montazer, M., 2016. Tunable shaped N-doped CuO nanoparticles on cotton fabric through processing conditions: synthesis, antibacterial behavior and mechanical properties. Cellulose 23 (3), 2229–2243.
Sedighi, A., Montazer, M., Hemmatinejad, N., 2014a. Copper nanoparticles on bleached cotton fabric: in situ synthesis and characterization. Cellulose 21 (3), 2119–2132.
Sedighi, A., Montazer, M., Samadi, N., 2014b. Synthesis of nano Cu2O on cotton: morphological, physical, biological and optical sensing characterizations. Carbohydr. Polym. 110, 489–498.
Shu, Y., Li, B., Chen, J., Xu, Q., Pang, H., Hu, X., 2018. Facile synthesis of Ultrathin nickel–cobalt phosphate 2D nanosheets with enhanced electrocatalytic activity for glucose oxidation. ACS Appl. Mater. Interfaces 10 (3), 2360–2367.
Süzer, S., 1997. Electron spectroscopic investigation of polymers and glasses. Pure Appl. Chem. 69 (1), 163–168.
Trchová, M., Stejskal, J., 2011. Polyaniline: the infrared spectroscopy of conducting polymer nanotubes (IUPAC Technical Report). Pure Appl. Chem. 83 (10), 1803–1817.
Wang, L., Lu, X., Wen, C., Xie, Y., Miao, L., Chen, S., Li, H., Li, P., Song, Y., 2015. One-step synthesis of Pt–NiO nanoplate array/reduced graphene oxide nanocomposites for nonenzymatic glucose sensing. J. Mater. Chem. 3 (2), 608–616.
Witkowska Nery, E., Kundys, M., Jeleń, P.S., Jönsson-Niedziółka, M., 2016. Electrochemical glucose sensing: is there still room for improvement? Anal. Chem. 88 (23), 11271–11282.
Yang, J., Jiang, L.-C., Zhang, W.-D., Gunasekaran, S., 2010. A highly sensitive non-enzymatic glucose sensor based on a simple two-step electrodeposition of cupric oxide (CuO) nanoparticles onto multi-walled carbon nanotube arrays. Talanta 82 (1), 25–33.
Yuan, B., Xu, C., Deng, D., Xing, Y., Liu, L., Pang, H., Zhang, D., 2013. Graphene oxide/nickel oxide modified glassy carbon electrode for supercapacitor and nonenzymatic glucose sensor. Electrochim. Acta 88, 708–712.
Zhan, B., Liu, C., Chen, H., Shi, H., Wang, L., Chen, P., Huang, W., Dong, X., 2014. Free-standing electrochemical electrode based on Ni (OH) 2/3D graphene foam for nonenzymatic glucose detection. Nanoscale 6 (13), 7424–7429.
Zhang, X., Sun, S., Lv, J., Tang, L., Kong, C., Song, X., Yang, Z., 2014. Nanoparticle-aggregated CuO nanoellipsoids for high-performance non-enzymatic glucose detection. J. Mater. Chem. 2 (26), 10073–10080.
Zhang, Y., Xu, F., Sun, Y., Shi, Y., Wen, Z., Li, Z., 2011. Assembly of Ni (OH) 2 nanoplates on reduced graphene oxide: a two dimensional nanocomposite for enzyme-free glucose sensing. J. Mater. Chem. 21 (42), 16949–16954.
Zou, Y., Wang, Q., Xiang, C., Tang, C., Chu, H., Qiu, S., Yan, E., Xu, F., Sun, L., 2016. Doping composite of polyaniline and reduced graphene oxide with palladium nanoparticles for room-temperature hydrogen-gas sensing. Int. J. Hydrogen Energy 41 (11), 5396–5404.